Journal of Zhejiang University-SCIENCE A (Applied Physics & Engineering) 2025 26(3):194-211
www.jzus.zju.edu.cn; www.springer.com/journal/11582
E-mail: jzus_a@zju.edu.cn

Research Article

https://doi.org/10.1631/jzus.A2400020

Evolution of waterproof performance, mechanical properties, and microstructure in hydrophobically-modified geopolymer concrete during dry-wet cycles

Dongming YAN[1], Yilu QIU[1], Rongfeng GAO[1], Shikun CHEN[1], Yi LIU[2], Shengqian RUAN[1]✉

[1]*College of Civil Engineering and Architecture, Zhejiang University, Hangzhou 310058, China*
[2]*School of Materials Science and Engineering, Zhejiang University, Hangzhou 310058, China*

Abstract: The waterproof performance, mechanical properties, chemical composition, microstructure, and pore structure of hydrophobically-modified geopolymer concrete are investigated before and after dry-wet cycles, to determine the long-term feasibility of using hydrophobically-modified geopolymer concrete in wet environments. We use two types of organic modifying agents: polydimethylsiloxane (PDMS) and sodium methyl siliconate (SMS). The experimental results show that incorporating 2%–6% PDMS or 5%–15% SMS can make the concrete hydrophobic, with water absorption and chloride transport rates decreasing by up to 94.3%. We also analyze the bonding modes of organic molecules and geopolymer gels, as well as their evolution mechanisms during dry-wet cycles. PDMS-modified geopolymer concrete is found to exhibit long-term waterproof performance that is not weakened by dry-wet cycles. This is attributed to the robust combination of organic components and the geopolymer gel skeleton formed through phase cross-linking. Meanwhile, PDMS-modified geopolymer concrete's hydrophobicity, strength, and microstructure are essentially unaffected. In contrast, SMS-modified geopolymer concrete shows higher water sensitivity, although it does maintain efficient waterproof performance. Due to relatively low binding energy, the dry-wet cycles may lead to the detachment of some SMS molecules from the gel network, which results in a decrease of 18.6% in compressive strength and an increase of 37.6% in total porosity. This work confirms the utility of hydrophobically-modified geopolymer concrete as a building material for long-term service in wet environments, for instance, areas with frequent precipitation, or splash and tidal zones.

Key words: Geopolymer concrete; Hydrophobic modification; Waterproof performance; Mechanical property; Microstructure analysis

1 Introduction

Geopolymers are innovative cementitious materials with high mechanical strength and workability (Wu et al., 2019). The aluminosilicate precursor materials used for synthesizing geopolymers are usually industrial by-products, or relatively inexpensive cementitious materials such as fly ash, slag, and metakaolin (MK). This results in significantly lower production energy consumption and carbon emissions compared to ordinary Portland cement production (Davidovits, 1989; Fletcher et al., 2005; Duxson et al., 2007; Provis and Bernal, 2014). Furthermore, appropriately mixed geopolymers exhibit superior performance to traditional cement in terms of early strength, thermal stability, and microstructure, making them attractive as high-performance building materials (Khale and Chaudhary, 2007; Provis and van Deventer, 2009; Zhong et al., 2022a). Despite the numerous favorable properties of geopolymers, their large-scale adoption in industry has been limited thus far. On one hand, due to the relatively short development history, there exists a dearth of comprehensive and long-term performance monitoring data to verify the durability of geopolymer concrete (Law et al., 2015; Amran et al., 2021). Investigation into the mechanical properties and corrosion resistance of geopolymers exposed to dry-wet cycles in wet and marine environments are comparatively scant. On the

✉ Shengqian RUAN, shengqian_ruan@zju.edu.cn
Dongming YAN, https://orcid.org/0000-0003-2522-3342
Yilu QIU, https://orcid.org/0009-0007-8304-949X

Received Jan. 12, 2024; Revision accepted May 8, 2024; Crosschecked Feb. 27, 2025

other hand, the existence of a substantial quantity of uncondensed hydroxyl groups in geopolymer matrix, coupled with the rich capillary pore structure, imparts conventional geopolymers with remarkable hydrophilicity and water absorption (Duxson et al., 2007; Chen et al., 2022).

The water resistance of building materials, such as geopolymers, in wet environments is important for maintaining long-term structural stability (Amran et al., 2021; Pradhan et al., 2022). Buildings located in environments with heavy rainfall, or hydraulic engineering structures are at risk of water leakage without adequate waterproofing measures, which can cause safety issues and economic losses. For structures located in marine environments with splash and tidal zones, such as bridges and docks, water intrusion can also transport soluble corrosion ions such as chloride and sulphate ions into concrete structures, leading to deterioration (Bakharev, 2005; Kou and Poon, 2013; Zhang P et al., 2018; Wang et al., 2019; Fu et al., 2021; Wasim et al., 2021). Consequently, it is imperative to develop geopolymer materials with low water adsorption and transport properties, which can enhance the durability of buildings in environments with alternating wet and dry conditions.

Recently, we synthesized hydrophobically-modified geopolymer pastes with low water absorption and excellent mechanical strength by incorporating two distinct organic liquids, polydimethylsiloxane (PDMS) and sodium methyl siliconate (SMS), into fresh MK-based geopolymer pastes (Ruan et al., 2021, 2023c). PDMS is a stable oily liquid composed of chain siloxane with numerous methyl groups (Zhong et al., 2022b). Due to the presence of these hydrophobic groups ($–CH_3$), PDMS has a low surface energy. Additionally, studies have shown that PDMS can directly modify the surface chemistry of geopolymer gels (Ruan et al., 2021, 2022b). The multi-sized micro papillary formed by the hybridization of PDMS can also increase the surface roughness and improve the hydrophobicity of geopolymers. Due to the hydrophobic layer attached to the matrix, the upward suction force exerted by the capillary walls on water is greatly reduced. Consequently, PDMS-modified geopolymer materials show low water absorption (Ruan et al., 2022a). Researchers also showed that the addition of 4% PDMS in slag/clay-based geopolymers can lead to a water contact angle of approximately 120°, and that the 2-h water absorption decreases by up to 75% (Zhong et al., 2022b). PDMS-modified alkali-activated slag exhibits excellent water repellence and low surface energy (Tang et al., 2023). The incorporation of PDMS can enhance the hydrophobicity of fly ash/slag-based geopolymers, raising the water contact angle from 57.32° to 127.64°, and reducing water absorption from 6.96% to 1.61% (Zhang et al., 2023).

In contrast, SMS is a micro-molecular organosilicone compound that can be hydrolyzed in alkaline solutions to form silanol structures, which may participate in the synthesis of geopolymers (Lv et al., 2022). The hydrophobic modification of geopolymers by incorporating SMS is attributed to the chemical grafting of organic methyl groups onto alkylated sodium aluminosilicate hydrate gels (Ruan et al., 2023b). Lu et al. (2023) reported that modified MK/fly ash-based geopolymer with 1.5% (mass fraction) SMS has a high water contact angle of 134.5°, and that its density, hardness, and wear resistance are all improved. Further studies showed that other micro-molecular organosilicones that contain hydrophobic structures, such as alkyl groups and carbon chains, have the capability of making geopolymers hydrophobic and waterproof (Lv et al., 2022; Zhang et al., 2022; She et al., 2023).

Our previous research found that the incorporation of PDMS and SMS can also reduce the early-stage shrinkage of MK-based geopolymer, and reduce the structural stress generated by unsaturated water inside the material (Ruan et al., 2023a). Nevertheless, research on geopolymers after hydrophobic modification with PDMS or SMS has primarily focused on synthesis methods or performance analysis within laboratory settings. There is a lack of study on modified geopolymers used in real building materials, and their suitability for engineering applications. In particular, it is important to investigate the mechanical properties, durability, and microstructural changes of concrete with modified geopolymers acting as binders in natural environments. Current research has shown that hydrophobic modification treatment can reduce the rate and severity of damage to concrete during freeze-thaw cycles (Zhong et al., 2023). However, the long-term waterproofing effect of PDMS- and SMS-modified geopolymer concrete has not yet been studied. Notably, moisture intrusion may interfere with or even strip away the organic components attached to the geopolymer matrix or aggregate, rendering the modified concrete non-functional.

In this work, we investigate the water absorption and chloride transport of PDMS- and SMS-modified MK-based geopolymer concrete, and compare the evolution of its waterproof performance, wettability, chemical composition, microstructure, and pore structure before and after dry-wet cycles. Specifically, our dry-wet cycles involve 12 h of water absorption and 12 h of gentle drying. These dry-wet cycles not only simulate frequent periodic precipitation, but also simulate tidal effects and wave attacks in coastal engineering applications (Banić et al., 2005; Artigas et al., 2015; Xie et al., 2019). The potential bonding mechanisms of PDMS and SMS molecules with geopolymer gels, and their evolution during dry-wet cycles are further discussed. We evaluate the feasibility of hydrophobically-modified geopolymer concrete as a building material for long-term service in engineering applications, laying a foundation for subsequent research and application.

2 Materials and experimental methods

2.1 Materials

Geopolymer concrete samples were prepared by mixing geopolymer binder, sand, and coarse aggregate (CA). MK, sodium silicate (SS) solution, and sodium hydroxide (SH) solid were used to synthesize the geopolymer binder. MK, which acts as the aluminosilicate precursor, was obtained from BASF SE (Germany) with the specific oxide composition presented in Table 1. The alkali activator solution consisted of SS solution (Hengli Chemical Ltd., China) and solid SH pellets (Sinopharm Chemical Reagent Co., China). The chemical composition of the SS solution was 26.0% of SiO_2, 8.2% of Na_2O, and 65.8% of water (mass fraction). The purity of SH pellets was ≥96%. The sand used in this study was obtained from Xiamen Elio Standard Sand Co. (China), and had a particle size of <2 mm. The grain composition of standard sand belongs to the second region of grading. The CA used to produce concrete samples was sourced from Nine-seven Building Materials Co. (China), and had a particle size ranging from 5 to 10 mm. The moisture contents of the standard sand and CA were approximately 4%.

Table 1 Oxide composition of metakaolin

Composition	Mass fraction (%)	Composition	Mass fraction (%)
SiO_2	54.25	Na_2O	0.29
Al_2O_3	42.45	K_2O	0.15
TiO_2	1.87	MgO	0.14
CaO	0.07	P_2O_5	0.09
Fe_2O_3	0.48	Other	0.21

PDMS and SMS were used as organic agents to modify the geopolymer concrete. PDMS, with a viscosity of 50 mm^2/s was a colorless and transparent oily liquid (Shanghai Xianding Biotechnology Co., China). SMS was a white solid powder and was slightly soluble in water (Jinan Xingchi Chemical Co., China). The solid content of SMS was ≥98%, and the silicone content was approximately 70%.

2.2 Sample preparation

Table 2 lists the mixture proportions employed for three types of geopolymer concrete samples, informed by previous studies (Ruan et al., 2022a, 2023a): ordinary geopolymer concrete (OGC) without any additives, PDMS-modified geopolymer concrete (PGC), and SMS-modified geopolymer concrete (SGC). The OGC sample was synthesized by mixing MK, SS, SH, water, sand, and CA. The PGC samples with designations of PGC2, PGC4, and PGC6 represented the geopolymer concrete including 2, 4, and 6 g of PDMS per 100 g of MK, respectively. Similarly, the sample designations of SGC5, SGC10, and SGC15 were assigned to SGC samples incorporating 5%, 10%, and 15% of

Table 2 Mixture proportions of OGC, PGC, and SGC samples

Sample designation	Mass (g)								$n(SiO_2$ in SMS)/ $n(SiO_2$ in SS) (%)
	MK	SS	SH	SMS	PDMS	Water	Sand	CA	
OGC	100	175.5	18.4		–	1.1	200	400	
PGC2	100	175.5	18.4		2	2.3	200	400	
PGC4	100	175.5	18.4		4	3.7	200	400	
PGC6	100	175.5	18.4		6	4.9	200	400	
SGC5	100	156.3	10.9	10.8		11.6	200	400	5
SGC10	100	137.0	8.2	21.7		25.2	200	400	10
SGC15	100	117.8	5.5	32.5		38.9	200	400	15

SMS as the SiO_2 substitution, respectively. In this work, the substitution rate of SMS indicates the proportion of SiO_2 in SMS that replaced SiO_2 in SS. To ensure comparability across the samples, the total water content (13%, mass fraction), Si-Al-Na molar ratio (2:2:1), and MK-sand-CA mass ratio (1:2:1) of all concrete samples were held the same.

As shown in Fig. 1, the preparation processes of the OGC, PGC, and SGC samples were slightly different. For the OGC sample, SH pellets and SS solution were first mixed thoroughly and cooled to room temperature to prepare an alkali activator (AA) solution. MK and AA were then poured into the JJ-5 cement mixer (purchased from Wuxi Jianyi Experiment Instrument Co., Ltd., China) and mixed at a slow speed of 140 r/min for 60 s, and then a high speed of 285 r/min for 60 s, resulting in the formation of a fresh and homogeneous geopolymer binder. For PGC samples, PDMS was added to the AA solution before mixing with solid materials. The oil-water suspension was highly agitated by a hand-held electric stirrer at 900 r/min for 3 min to fully emulsify the PDMS in the AA solution. For SGC samples, SMS powder was incorporated into the AA solution and stirred at 60 r/min for 3 min with a stirring rod until the solid powder was completely dissolved. Once the fresh geopolymer binder was prepared, it was poured into a concrete mixer along with standard sand and CA. After 5 min of mixing, the concrete was then poured into molds with dimensions of 50 mm×50 mm×50 mm, wrapped with plastic films, and placed in a standard curing room under controlled conditions (temperature: (20±2) °C, relative humidity (RH): about 98%). After 1 d of curing, the concrete samples were demolded and then cured further in the standard curing room for another 27 d.

2.3 Methods

2.3.1 Water absorption test

In accordance with the standard SL/T 352-2020 (MWRC, 2020), the water absorption behaviors of 28-d cured concrete samples were monitored by gravimetry. Before the test, the concrete samples were subjected to a drying period at a controlled temperature of (40±5) °C for 108 h. To prevent moisture absorption, five surfaces of each 50-mm cubic sample were coated with paraffin wax. The single untreated surface of each concrete sample was immersed into distilled water with a depth of approximately 10 mm for the water absorption test. The mass gain of the samples was measured every day to calculate water absorption. The solution was replaced on a weekly basis.

2.3.2 Chloride transport depth measurement

The chloride transport depth measurement was used to briefly characterize the chloride transport in modified concrete samples (Fig. 2). The silver nitrate ($AgNO_3$) solution was used as a chromogenic reagent

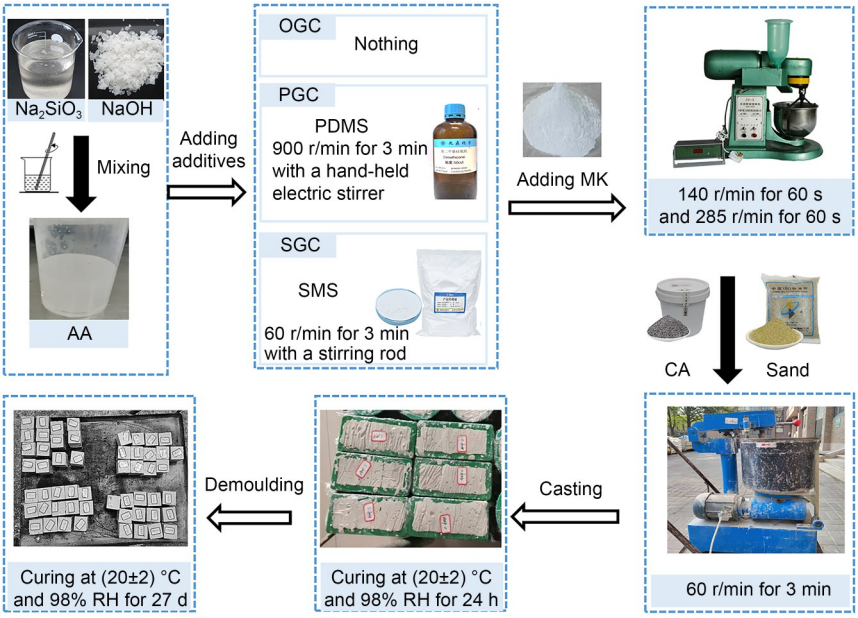

Fig. 1 Preparation processes of OGC, PGC, and SGC samples

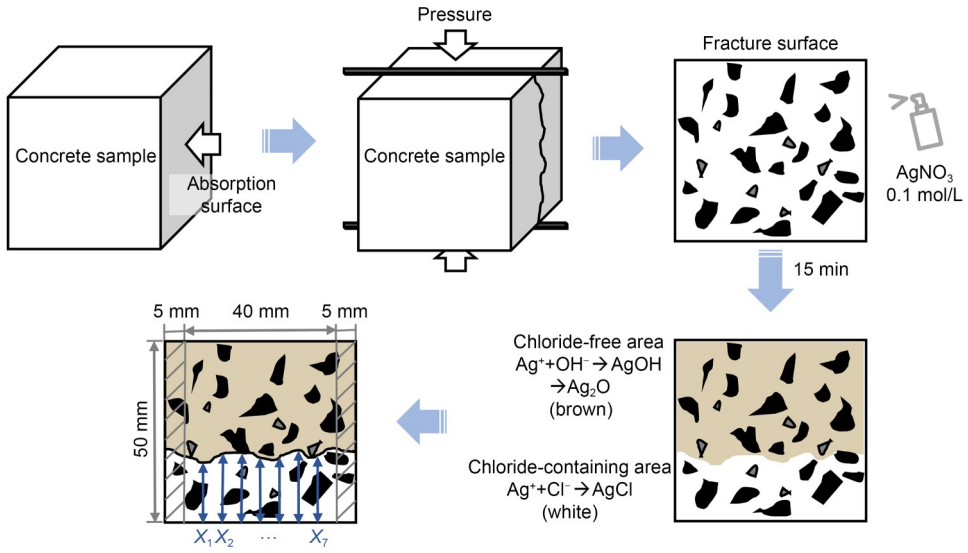

Fig. 2 Measurement procedure for chloride transport depth in geopolymer concrete samples. References to color refer to the online version of this figure

to visualize areas of chloride permeation (Baroghel-Bouny et al., 2007). As informed by recent studies (Li et al., 2021; Tomar et al., 2023), the concrete samples, after curing for 28 d, were immersed in 3.5% NaCl solution for durations of 1, 3, 7, 14, and 28 d. Upon reaching the designated times, the samples were removed and split along the radial direction. $AgNO_3$ solution with a volume of (1.5±0.3) mL and a dosage of 0.1 mol/L was then sprayed evenly onto the fracture surface of the concrete samples. These samples were left undisturbed for around 15 min to allow for color development. Subsequently, two distinct areas of white and brown appeared on the fracture surface, with a clear boundary between them. The depth of the white area was typically considered as the chloride penetration depth, while the brown area was considered the region without chlorides. Referring to the standard NT Build 492 (NCF, 1999), the average depth of the white area on the fracture surface was calculated as follows: (1) The transport depth was measured by assessing the distance from the center to both sides at 5 mm intervals. A total of seven data points were obtained and labelled as X_1 to X_7. (2) The average value, denoted as X_d, was determined from a set of seven data points (from X_1 to X_7), representing the depth of chloride transport.

2.3.3 Dry-wet cycles

To assess the long-term waterproof performance of modified concrete, dry-wet cycles representing the environmental conditions encountered by buildings in tidal zones were simulated. According to the standard GB/T 11969-2020 (SAC, 2020), the change in water content of samples during dry-wet cycles was measured, and the evolutions in their properties were compared. After pre-drying at a temperature of (40±5) °C for 108 h, the concrete samples underwent a series of dry-wet cycles as follows: (1) The dried samples were cooled naturally to (20±5) °C at room temperature (for around 30 min) to minimize the effect of the temperature change on the water absorption process. (2) The cooled samples were completely immersed in water for about 12 h. (3) Subsequently, the samples were removed from the water and allowed to dry naturally at room temperature for a period of 30 min, which minimized potential structural damage caused by surface water loss during the rapid drying process. (4) The samples were then placed in an oven with a temperature of (40±5) °C and dried for around 12 h, thereby completing one dry-wet cycle. The weight of the samples was recorded after each drying and wetting stage. In total, 32 dry-wet cycles were performed.

2.3.4 Water contact angle test

The water contact angle was measured using the Dropmeter 100P (Haishumaishi Detection Technology Co., Ltd., China) to evaluate the static wettability of the geopolymer matrix before and after dry-wet cycles. The water contact angle could be directly obtained by measuring the angle between the tangents of the

solid-liquid and liquid-gas interfaces. To eliminate the interference of large-size CA on the water contact angle measurement, the geopolymer matrix was extracted from concrete samples for wettability characterization. The crushed concrete was sieved with 50-mesh (0.282 mm) and 200-mesh (0.075 mm) sieves sequentially. Considering that approximately 20% of standard sand particles are smaller than 0.3 mm, the powder obtained after sieving with a 50-mesh sieve was considered as the mortar mixture of geopolymer and sand powder. Powders passing through the 200-mesh sieve were considered as geopolymer matrix. These powders were dried at 40 ℃ for 8 h and subsequently compacted onto glass slides. To ensure accuracy, over six water contact angle tests were conducted for each sample, and outliers were excluded before calculating the average value.

2.3.5 Compressive strength measurement

Compressive strength is a common indicator of the degree of geopolymerization, and an important evaluator of the applicability of geopolymer concrete (Guo et al., 2010). Referring to standard GB/T 50107-2010 (MOHURD, 2020), we tested the compressive strength of 50-mm cubic concrete samples before and after dry-wet cycles using an Instron 8802 machine, with a loading speed of 2.0 kN/s.

2.3.6 Fourier transform infrared spectroscopy

Fourier transform infrared spectroscopy (FTIR) spectroscopy was used to analyze the chemical composition of the geopolymer matrix in concrete samples before and after dry-wet cycles. The FTIR spectroscopy instrument is a NICOLET iS50 FTIR spectrometer manufactured by Thermo Scientific Instruments (China), and has a resolution of 4 cm^{-1}. When infrared light is transmitted through a sample, each functional group resonates with its characteristic absorption frequencies of the spectra (Witkowski and Koniorczyk, 2018). The tested samples underwent pre-drying and then 32 d of drying. We normalized the recorded data before analysis.

2.3.7 Scanning electron microscopy

Scanning electron microscopy (SEM) test was performed to analyze the microstructure of concrete samples, using a desktop SEM device (Phenom-PROX, Phenom World BV Company, the Netherlands). Sample fragments with a size of approximately 5 mm and a flat surface were selected for the test. Platinum-coated samples were fixed on the test bench with conductive tape, and then the test chamber was vacuumed. The spectrum for each measurement point was collected over a 30 s period. The working distance was 10.5 mm, and the spot was held at 3.5.

2.3.8 Mercury intrusion porosimetry

Mercury intrusion porosimetry (MIP) was used to characterize the pore structure of the geopolymer matrix in concrete samples before and after dry-wet cycles. It was conducted using an AutoPore IV9500 automatic mercury intrusion porosimeter (Micromeritics Instruments Corp., USA). We selected and crushed blocks at the core of concrete samples for testing. After crushing, a 60-mesh sieve was utilized to eliminate CA particles. Remaining particles with a size of 2–3 mm were selected for the MIP test. Before the test, the samples were dried in an oven at 45 ℃ for 12 h. The measured pore sizes ranged from 5 nm to 355 μm.

3 Results

3.1 Waterproof performance

3.1.1 Water absorption behavior

Fig. 3 shows the variation of cumulative water absorption over 20 d for OGC, PGC, and SGC samples. The water absorption of each sample before water saturation is essentially proportional to the square root of time $t^{1/2}$, which conforms to Hall's model on the one-dimensional moisture absorption kinetics of porous solids (Hall, 1989). After 1 d of water absorption, the OGC has effectively been water saturated, and its cumulative water absorption is around 8.5%. In contrast, the water absorption rate of PGC and SGC samples incorporating PDMS and SMS is much slower than that of OGC. The water absorption coefficient S of PGC2, PGC4, PGC6, SGC5, SGC10, and SGC15 samples, which is represented by the slope of the cumulative water absorption function before water saturation, is decreased by 80.5%, 85.1%, 93.1%, 77.6%, 89.1%, and 94.3%, respectively, compared to that of OGC (Fig. 3). These results indicate that geopolymer concrete is effectively modified by these two organic additives, and it exhibits strong waterproof performance with a low water absorption rate in wet environments.

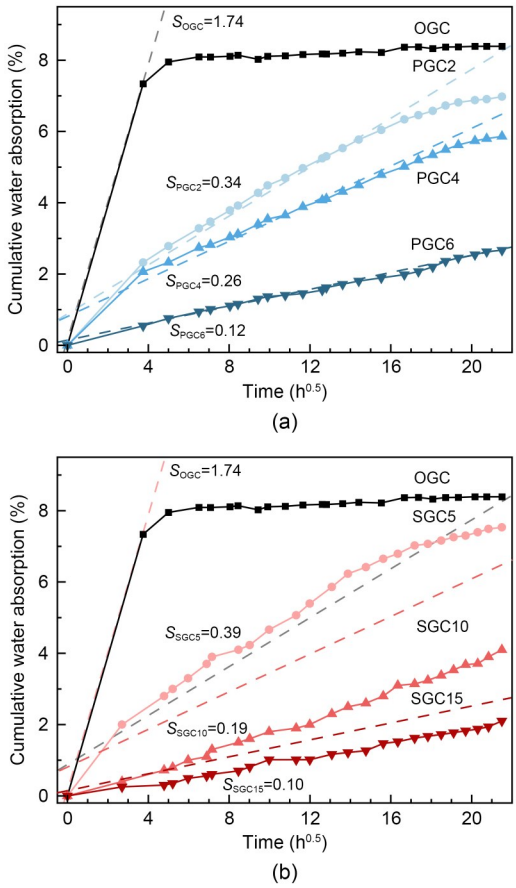

Fig. 3 Time-evolution of the cumulative water absorption of OGC and PGC samples (a) and OGC and SGC samples (b)

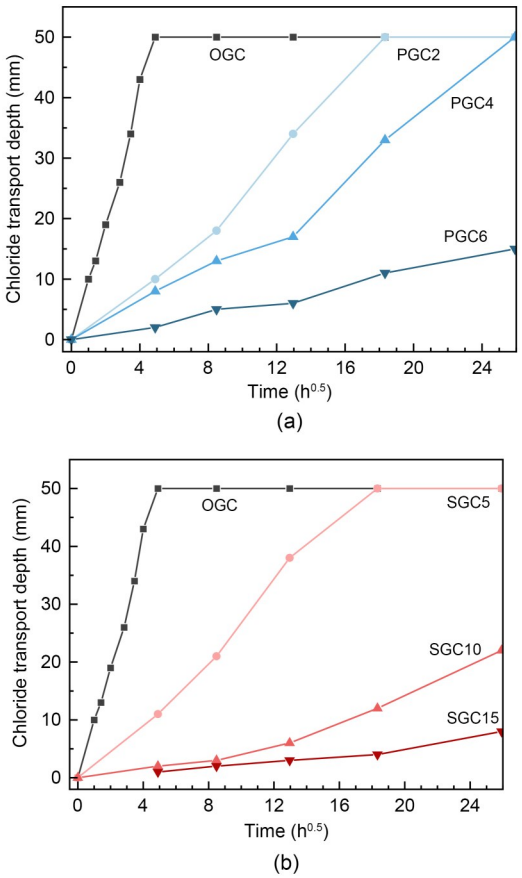

Fig. 4 Time-evolution of the chloride transport depth of OGC and PGC samples (a) and OGC and SGC samples (b)

3.1.2 Chloride transport depth

Fig. 4 depicts the variation of chloride transport depth in the OGC, PGC, and SGC samples during the one-dimensional NaCl solution absorption test. The goal of this test is to assess the preliminary corrosion resistance of modified concrete. Similar to the results of the water absorption test, the transport rate of chloride ions in SGC and PGC samples is much lower than that in OGC. Although the chloride ion has diffused to the top surface of OGC sample after 1 d (50 mm), the 28-d chloride transport depths of PGC6, SGC10, and SGC15 are only 15, 18, and 8 mm, respectively. This demonstrates that the waterproof modified concrete can also hinder the penetration and diffusion of corrosive chloride. The transport behavior of chloride ions is a complex process, which mainly depends on the ion concentration, the proportion of transport channels (continuous waterway), and the interaction force between pore walls and ions (Xue et al., 2018; Jin et al., 2023). In the initial stage of absorption, when the interior water content of the sample is low, chloride migration is primarily driven by the moisture gradient (Homan et al., 2016). As chloride transport continues, the concrete samples that are wettened by the solution start to undergo secondary penetration (Liu et al., 2020; Zhu et al., 2022). This study mainly focuses on the evolution of waterproofing performance, and chloride resistance is only briefly explored.

3.2 Water loss and absorption during dry-wet cycles

Fig. 5 illustrates the changes in the water content of OGC, PGC, and SGC samples during the dry-wet cycle test. The objective of this test is to explore the waterproof performance of modified concrete in engineering applications. Over the course of 32 cycles, the PGC samples maintain efficient water repellence. The average water content gains of OGC, PGC2, PGC4, and PGC6 samples through absorption were 7.1%, 5.6%, 5.0%, and 3.0%, respectively. Although SGC samples also show effective long-lasting waterproof

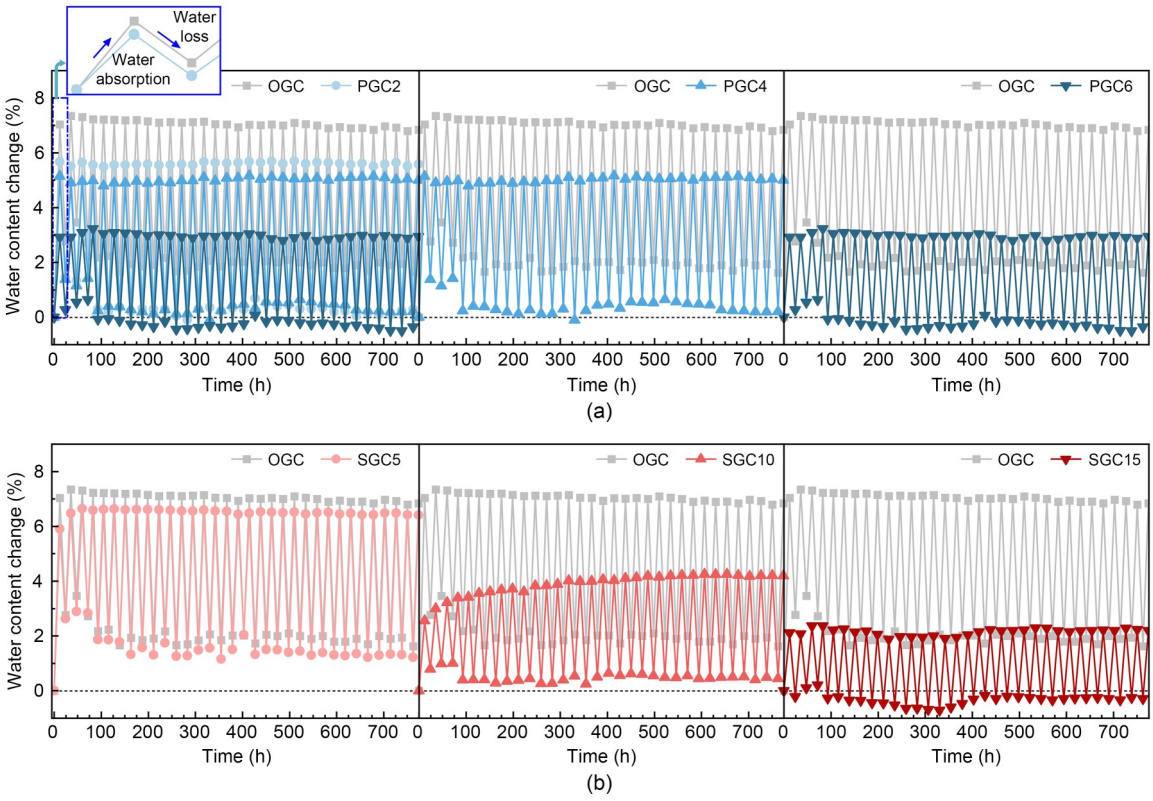

Fig. 5 Water content change of OGC and PGC samples (a) and OGC and SGC samples (b) during 32 dry-wet cycles. References to color refer to the online version of this figure

performance, the single water absorption contents of SGC5 and SGC10 samples exhibit an obvious increasing trend as the dry-wet cycle proceeds. As shown in Fig. 5b, the water absorption content in SGC5 increases from 5.9% to 6.6% in the first three cycles, and in SGC10 it increases from 2.5% to 4.0% in the first 14 cycles. The final water absorption contents remain at 6.5% for SGC5 and 4.1% for SGC10. These results indicate that the water loss-absorption process may interfere with cross-linking between organic SMS and inorganic concrete, or that this hybrid system can degrade during dry-wet cycles. However, the dry-wet cycles seem to have little impact on SGC15, as its water absorption content stays around 2.1%. In addition, the concrete samples exhibit distinct water loss behavior during dry-wet cycles. OGC cannot restore its original moisture content after a 12-h drying process, due to the high affinity between the moisture and the hydrophilic geopolymer matrix/aggregate (Parbhoo and Nagy, 1988). This phenomenon is particularly evident in the first three cycles, with a residual moisture content of 2.7%–3.5% after drying. Due to the barrier of the existing water film, the residual moisture content during the subsequent dry-wet cycle essentially remains constant at around 1.9%. In contrast, concrete samples with a sufficient dosage of hydrophobic agents (PGC2, PGC4, PGC6, SGC10, and SGC15) can be completely dried within 12 h. The mechanisms of moisture content and waterproof performance evolution during dry-wet cycles will be discussed further in subsequent sections.

3.3 Wettability changes

Fig. 6 presents the morphology of water droplets on the fracture surfaces of OGC, PGC6, and SGC15. We can see that overall, the PGC and SGC display strong hydrophobicity. Fig. 7 illustrates the morphology of water droplets on the geopolymer matrix powder,

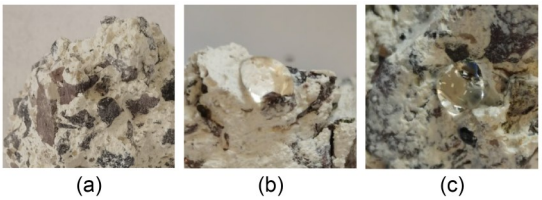

Fig. 6 Morphologies of water droplets on the fracture surfaces of (a) OGC, (b) PGC6, and (c) SGC15

as well as the mixture of sand and matrix powder (i.e., mortar powder) taken from original OGC, PGC, and SGC samples. The geopolymer matrix from PGC or SGC with an adequate quantity of PDMS or SMS exhibits greater hydrophobicity compared to that of OGC. It can be observed that the adsorption capacity of mortar powder to water (Fig. 7b) is significantly enhanced compared to that of matrix powder (Fig. 7a). When a water droplet fell on the mortar powder from PGC or SGC, it turned into a small oblate ball enveloped by sand and matrix powder. These results indicate that the two organic additives tend to adsorb or bond to the geopolymer matrix rather than become attached to the surface of sand. This is the reason why PGC and SGC samples maintain long-term waterproof performance through dry-wet cycles.

Fig. 8 shows the water contact angle of the pressed matrix powder from OGC, PGC, and SGC samples before and after dry-wet cycles. Before the dry-wet cycles, the water contact angles of the matrix powders from OGC, PGC6, and SGC15 are 34.7°, 136.7°, and 139.0°, respectively. Incorporating PDMS at a dosage of 2%, or substituting SMS at a rate of 5%, can prompt the originally-hydrophilic geopolymer matrix to become hydrophobic (when the water contact angle is greater than 90°). The results indicate that these organic components can reduce the surface energy of the geopolymer matrix, and perform hydrophobic modification of the inorganic material. PDMS and SMS molecules can be connected to geopolymer gels through physical adsorption or covalent bonds (Witkowski and Koniorczyk, 2018; Kang et al., 2022; Ruan et al., 2023c). After dry-wet cycles, the water contact angle of the matrix powder from all concrete samples decreases slightly by 0.4%–7.7%, which demonstrates that the dry-wet cycles have little impact on the apparent hydrophobicity of modified concrete. Therefore, PGC and SGC have reliable and long-lasting waterproof performance, ensuring effectiveness in engineering applications.

3.4 Compressive strength changes

Fig. 9 presents the values of compressive strength for OGC, PGC, and SGC samples before and after dry-wet cycles. Prior to dry-wet cycles, the original OGC sample exhibits a high compressive strength of 57.4 MPa. The addition of PDMS slightly reduces the compressive strength by values ranging from 1.5% to 5.7%. In contrast, the strengths of all PGC samples are still over 54 MPa, which may be due to the introduction of air bubbles inside the concrete caused by the PDMS (Wang et al., 2020). In the case of SGC samples, the addition of SMS leads to a significant decrease in compressive strength. The compressive strengths of 28-d cured SGC10 and SGC15 are 24.2% and 47.6% lower than that of OGC, respectively, suggesting that the small organosilicone-based SMS can weaken the originally-robust gel structure of geopolymers through chemical bonding (Lv et al., 2022; Ruan et al., 2023c). After the dry-wet cycles, both OGC and PGC samples show a slight decrease in compressive strength, being less than 2.3 and 1.5 MPa, respectively. The addition of PDMS slightly improves the stability and durability of geopolymer concrete in wet environments. In contrast, SGC samples show greater compressive strength changes during dry-wet cycles compared with PGC samples. The compressive strengths of SGC5, SGC10,

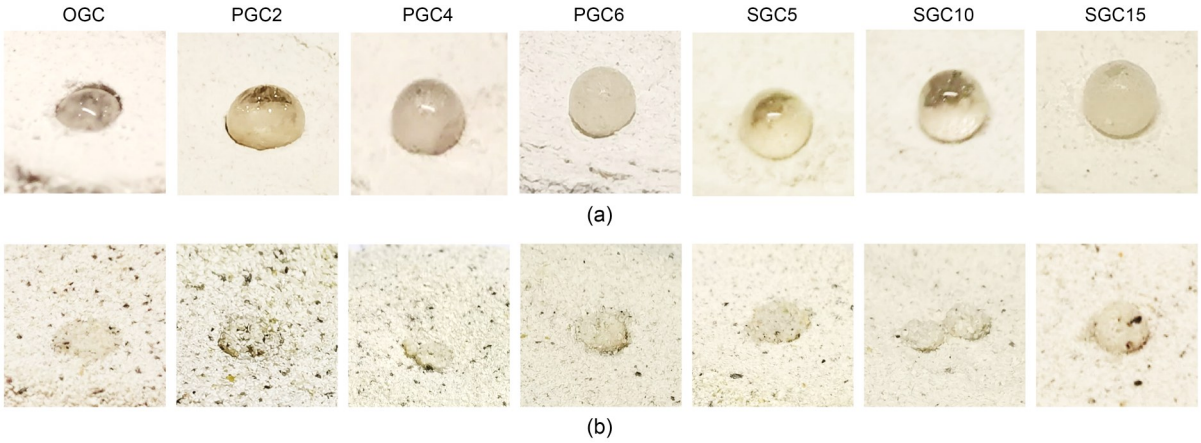

Fig. 7 Morphologies of water droplets on the surfaces of (a) the geopolymer matrix powder and (b) the mixture of sand and matrix powder (i.e. mortar powder) taken from original OGC, PGC, and SGC samples

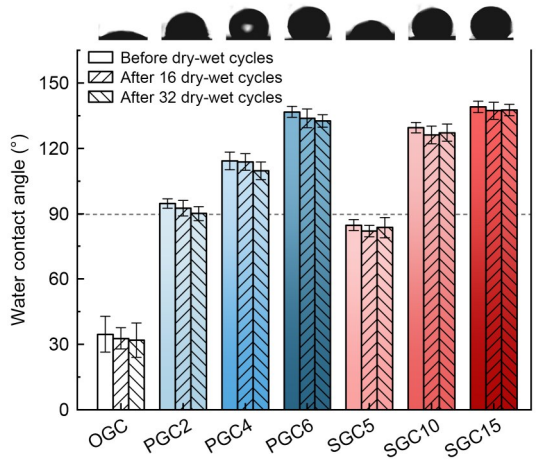

Fig. 8 Water contact angle of the pressed matrix powder from OGC, PGC, and SGC samples before and after dry-wet cycles

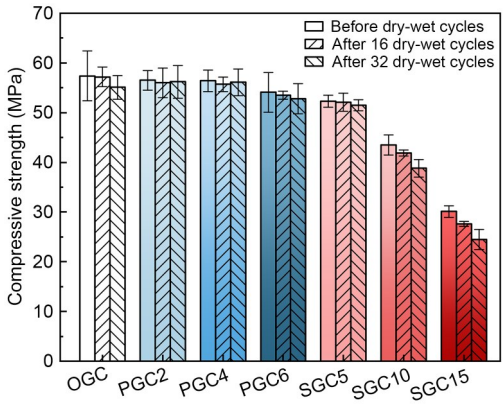

Fig. 9 Compressive strength of OGC, PGC, and SGC samples before and after dry-wet cycles

and SGC15 samples after 32 dry-wet cycles fall by 1.5%, 10.8%, and 18.6%, respectively, compared to OGC. The geopolymer matrix grafted with SMS apparently has higher sensitivity to internal moisture transport. This is likely related to the binding state of the organic-inorganic components, and will be discussed later.

3.5 Chemical composition evolution

Fig. 10 displays the FTIR spectra of the geopolymer matrix from OGC, PGC4, and SGC10 samples in the range of 500–4000 cm^{-1}, before and after dry-wet cycles. The change in the wavenumber of the main band is an indicator of aluminosilicate dissolution and gel formation. Before dry-wet cycles, the main absorption band of OGC and PGC appears at 1017 cm^{-1}, while that of SGC appears at 1028 cm^{-1}, revealing that SMS

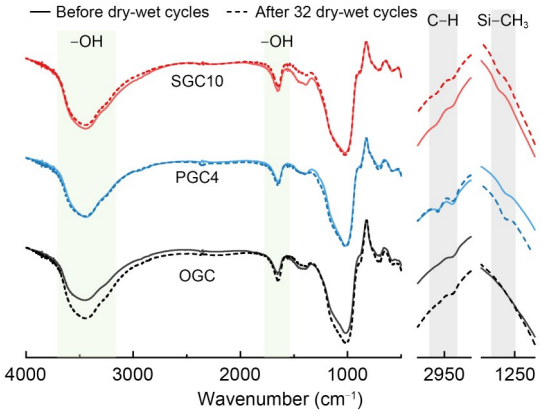

Fig. 10 FTIR spectra of geopolymer matrix from OGC, PGC4, and SGC10 samples before and after 32 dry-wet cycles

directly affects the formation of aluminosilicate gels in geopolymer concrete. All three FTIR curves of samples before dry-wet cycles show intense absorption bands at around 1000 and 450 cm^{-1}, which are attributed to the asymmetric stretching and bending vibrations of Si–O–T (T: Si or Al), respectively (Xue et al., 2018; Lu et al., 2023). After 32 dry-wet cycles, the FTIR pattern of each type of concrete at approximately 1000 cm^{-1} is essentially the same as that of the original concrete, indicating that the influence of dry-wet cycles on the gel-level structure (<1 nm) in geopolymer concrete is negligible. The peaks at the wavenumbers of approximately 2950 and 1280 cm^{-1}, which correspond to the vibrations of organic structures C–H and Si–CH_3, respectively, are still present without distinguishable weakening. This is a key indicator of the ability of the modified concrete to maintain waterproof performance despite continued moisture intrusion (Chandler, 2002). Moreover, due to moisture retention after incomplete drying for the OGC sample, its absorption peaks at 1650 and 3500 cm^{-1} are significantly enhanced due to hydrogen bonding between Si–OH on inorganic gels and adsorbed water, as well as elongation of the O–H bonds in Si–OH (Zhang ZH et al., 2018). In contrast, hydrophobic PGC and SGC samples just weakly bind to water molecules, so the vibration amplitudes of peaks representing –OH are basically the same as in the original samples.

3.6 Microstructure evolution

As shown in Fig. 11, SEM images (scaled up by 4000) showcase the micron-scale morphology of OGC, PGC4, and SGC10 samples before and after dry-wet

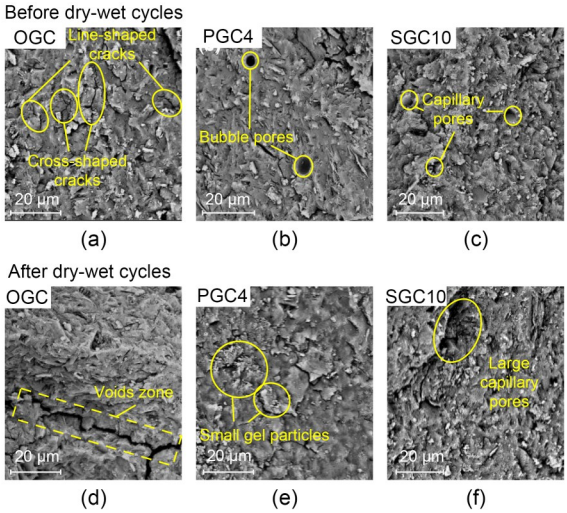

Fig. 11 SEM images (×4000) of OGC, PGC4, and SGC10 samples (a–c) before and (d–f) after 32 dry-wet cycles

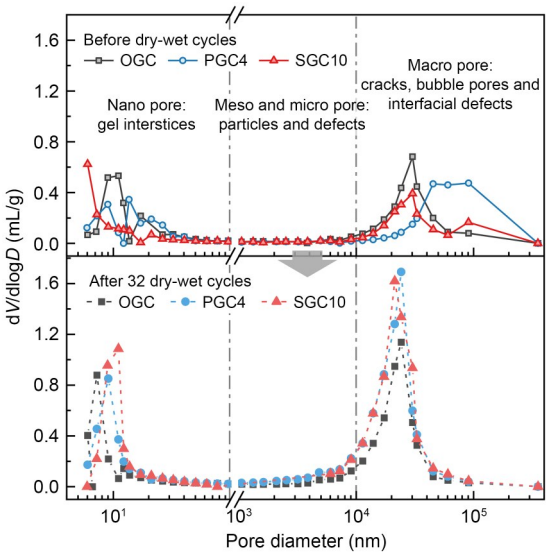

Fig. 12 Pore size distribution of geopolymer matrix from OGC, PGC4, and SGC10 samples before and after 32 dry-wet cycles

cycles. Prior to the dry-wet cycles, the structures of the three samples are relatively dense. In these structures, there are some small line-shaped and cross-shaped cracks with lengths around 10–20 μm in the matrix of the OGC sample (Zhu et al., 2023). In the PGC sample, spherical bubble pores with smooth pore walls are clearly visible, which were introduced during the preparation process (Ruan et al., 2021). Moreover, the SGC sample has more micron-level capillaries, which are irregularly shaped and filled with some small gel particles. After dry-wet cycles, all three samples show a certain degree of deterioration in their matrix. The presence of pores and micro-cracks in the OGC sample increases, possibly due to greater shrinkage during the dry-wet cycles. There is no distinguishable increase in the presence of cracks in the PGC sample, which is attributed to the stable gel structure and waterproof capability. In contrast, the micron-scale defects and pores in the SGC sample apparently become more numerous and larger after dry-wet cycles, which is possibly due to the degradation of matrix components in SGC.

3.7 Pore structure evolution

The pore structure was characterized using the MIP technique, to further analyze the microstructural evolution of the geopolymer concrete. Fig. 12 shows the pore size distribution of geopolymer matrix from OGC, PGC4, and SGC10 samples before and after dry-wet cycles. The pore sizes of all samples are mainly concentrated at 5–40 nm and 10–200 μm, which correspond to gel interstices, and large defects (e.g. cracks, bubbles, and interfacial defects), respectively (Chen et al., 2022). As seen in Fig. 13, the total porosity (measuring range: 5 nm–355 μm) and porosity of pores in different sizes of OGC, PGC4, and SGC10 matrix are calculated and compared. Before dry-wet cycles, the total porosity of the OGC matrix is 43.2%, and the addition of 4% PDMS and the replacement of 10% SMS led to an increase of 22.0% and a decrease of 9.0%, respectively (Fig. 13a). The addition of PDMS predominantly increases the cumulative volume of large-sized bubble pores, and the porosity of pores larger than 10 μm in PGC4 is 12.9% higher than that in OGC (Fig. 13f). However, more small gel pores are created in the SGC matrix (Fig. 13b), which again proves that SMS molecules can participate in geopolymerization reactions and alter the gel structure of geopolymers. It is worth noting that a large number of the smallest detectable pores are found in the SGC10 matrix, so one can speculate that many pores smaller than 5 nm also exist in this system (Fig. 12).

After 32 dry-wet cycles, the total porosities of the OGC, PGC4, and SGC10 matrices increase by 11.8%, 12.9%, and 37.6%, respectively (Fig. 13a). Dry-wet cycles can cause a certain degree of matrix structure degradation in all samples, and its effect is the most significant on SGC. As shown in Fig. 13f, the porosity of macro-scale pores in SGC10 increases by over 54% after dry-wet cycles, but that of PGC4 remains basically unchanged. This is also an important reason why

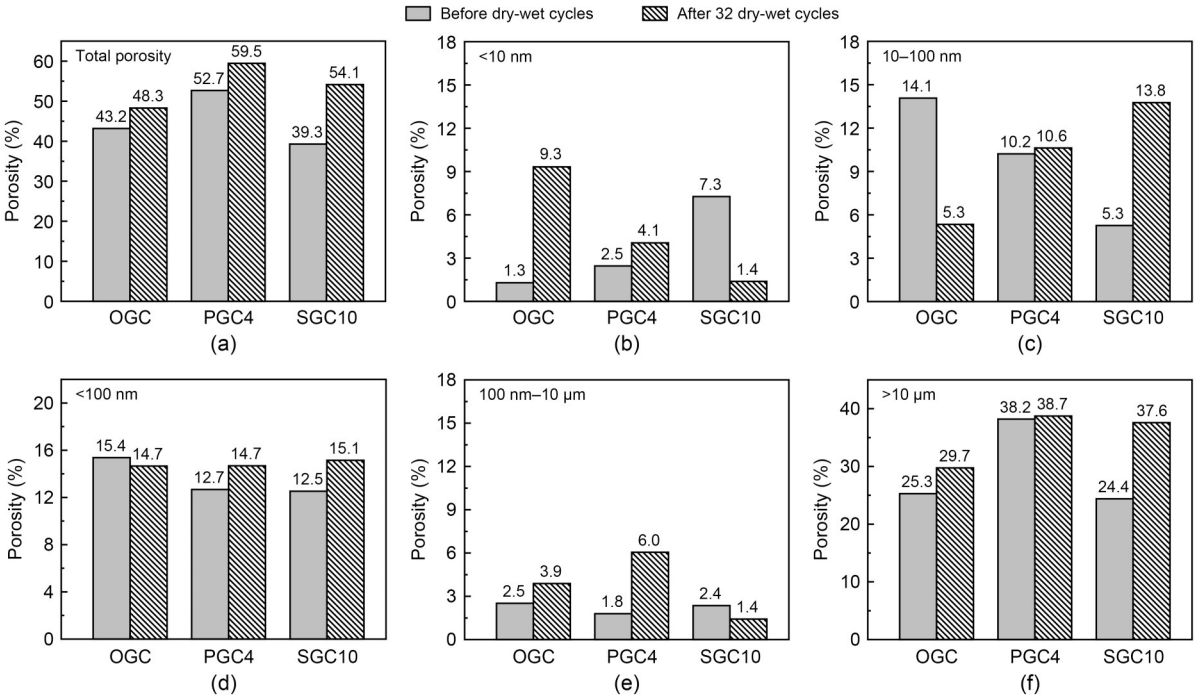

Fig. 13 Porosity of pores of different sizes in geopolymer matrix from OGC, PGC4, and SGC10 samples before and after 32 dry-wet cycles: (a) total porosity; (b) <10 nm; (c)10–100 nm; (d) <100 nm; (e) 100 nm–10 μm; (f) >10 μm

the waterproof performance and strength of SGC are gradually weakened during dry-wet cycles (Fig. 5). In addition, the porosity for nano-scale pores (<100 nm) in all samples after dry-wet cycles only changes slightly (<2.6%, Fig. 13d). However, the variations in pore size for different samples exhibit different trends (Figs. 13b and 13c). For OGC, a proportion of the larger pores (10–100 nm) evolve into smaller pores of size <10 nm. This result may be attributed to the continuous generation of geopolymer gel, which fills these pores during dry-wet cycles (Provis and van Deventer, 2009). In contrast, the nano-scale pores in SGC10 matrix show a significant size increase after dry-wet cycles, with the porosity of pores of size 10–100 nm rising by 160.4%. Although meanwhile, the porosity of pores of size <10 nm falls by 80.8%. The large-sized capillary pores display stronger capillary pressures and suction for water, so their increase can enhance the volume shrinkage and water absorption of SGC samples (Neithalath et al., 2010; Chen et al., 2022; Peng et al., 2022).

4 Discussion

Fig. 14 showcases the potential bonding modes between the organic component and the gel skeleton in geopolymers, and their evolution mechanisms during dry-wet cycles. For OGC samples, the geopolymer wraps sands and CA into a uniform system. The capillary pores in the geopolymerization-synthesized matrix and the interfacial voids between the paste and aggregate are the main channels for moisture transport in concrete (Babaee and Castel, 2018; Tian et al., 2023). Capillary pores are usually considered to be pore structures with a size of 10 nm–10 μm (Chen et al., 2022). The water diffused in the capillary pores can slowly fill nano-scale pores, with a size smaller than 10 nm, through secondary flow (Villagrán Zaccardi et al., 2017). Since the water absorption time for the dry-wet cycles in this study was short (12 h), most of the absorbed water fills the capillary pores and larger gel pores in the geopolymer concrete (Fig. 14a). During the drying process at 40 °C, most of the liquid water in the pores escapes the concrete via water vapor evaporation. However, given the high binding energy between the surface water film and the gel skeleton via hydrogen bonding, the elevated temperature-induced driving force cannot displace all water molecules from the geopolymer matrix (Sun et al., 2021). Consequently, OGC samples contain about 2% residual water after the drying process in dry-wet cycles (Fig. 5). The evaporative loss of water also intensifies the drying shrinkage of the

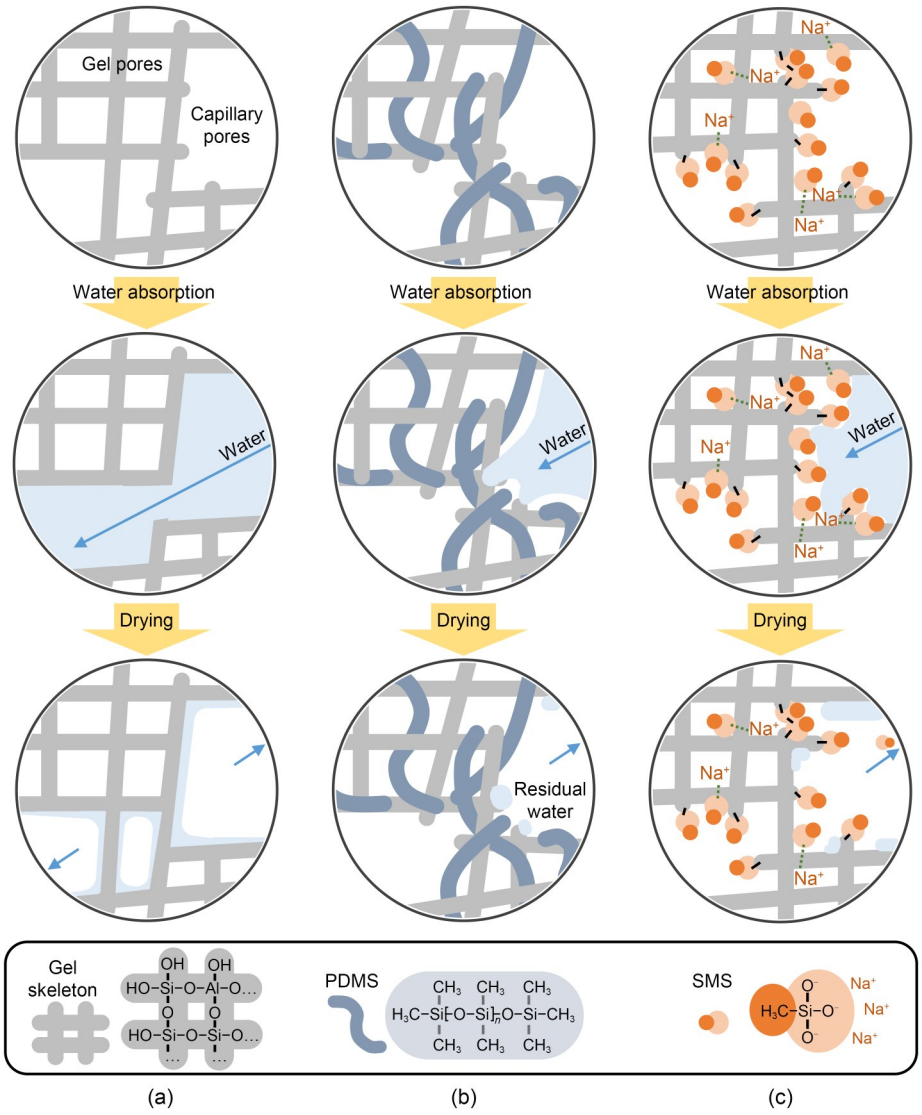

Fig. 14 Schematic of potential bonding modes of PDMS and SMS molecules with geopolymer gels and their evolution mechanisms during dry-wet cycles

geopolymer matrix, and causes micro-cracks to develop. Therefore, the total porosity of the OGC sample increases after a dry-wet cycle. The evaporative loss of water also intensifies the drying shrinkage of the matrix and promotes the development of micro-cracks (Mastali et al., 2018). Thus, the total porosity of the OGC sample increases after a dry-wet cycle (Fig. 13a).

The effective long-term waterproof performance of the two geopolymer concretes modified by PDMS and SMS can be attributed to the consistent presence of hydrophobic functional groups within the matrix, rather than in the pore structure. Nevertheless, differences in molecular structure give rise to distinctions in the bonding modes of PDMS and SMS with geopolymer gels, as well as differences in their evolution during dry-wet cycles. As seen in Fig. 14b, PDMS, as an organic polymer, has a stable long-chain molecular structure, which can form a uniform hybrid system with the inorganic gel skeleton through phase cross-linking. In contrast, it generally cannot form chemical bonds with the gel (Tang et al., 2023). In PGC, PDMS with hydrophobic methyl groups exposed on the surface of capillary pores reduces the channels' suction of water, thereby decreasing the water absorption rate of PGC (Ruan et al., 2022a; Zhong et al., 2022b). For similar reasons, the PGC systems contain less residual water and show less shrinkage after drying processes, leading to a more stable pore structure (Fig. 13). It is

worth noting that the combination of PDMS and gel skeleton is hardly affected by dry-wet cycles. This is attributed to the stable and completely hydrophobic molecular structure of PDMS, which allows PGC to maintain long-term and efficient waterproof performance.

In contrast, SMS micro-molecules feature hydrophobic methyl groups and reactive silanol structures, which can be combined with geopolymer gel structures in multiple modes (Fig. 14c) (Lu et al., 2023). During the geopolymerization process, a portion of SMS can form strong covalent bonds through dehydration condensation with hydroxyl groups on the surface or endpoints of gel particles (Lv et al., 2022). Negatively charged SMS monomers can also bind within the matrix through electrostatic attraction with sodium ions in the gel network. In addition, SMS can be physically adsorbed on inorganic gels because its silanol structure is hydrophilic. In a system with sufficient SMS, the SMS molecules that are grafted or adsorbed onto the gel can also form a dense hydrophobic network through self-condensation to envelop the gel skeleton. This leads to modified SGC having excellent hydrophobicity and water resistance (Yang et al., 2021; She et al., 2023). However, the bonding energies of van der Waals forces and electrostatic attraction are relatively lower than those of covalent bonds (Israelachvili, 1974).

Throughout dry-wet cycles of SGC samples, a proportion of the SMS molecules, initially adsorbed onto geopolymer gels through weak binding, establish more robust hydrogen bonds with water molecules, thereby dissolving in the water and being transported along with it (Zhang et al., 2022). The hydrophilic matrix where the hydrophobic SMS molecules were originally attached is re-exposed, facilitating the adsorption of residual water. This is also the reason why SGC5 and SGC10 samples show obvious increases in absorbed water content during the dry-wet cycles (Fig. 5b). For the SGC15 sample, because a substantial amount of SMS is chemically condensed and immobilized onto the gel surface, the loss of a small quantity of adsorbed SMS molecules cannot cause the exposure of matrix sites. Consequently, the water absorption of the SGC15 sample remains almost unchanged during dry-wet cycles. Notably, the detachment of SMS molecules from the gel network can result in structural damage to the matrix. This process causes the gel pores of SGC to enlarge, and leads to a significant increase in macro-scale defects, total porosity, and strength.

5 Conclusions

We have investigated the evolution of the waterproof performance, mechanical properties, chemical composition, microstructure, and pore structure of hydrophobically-modified geopolymer concrete incorporating PDMS (i.e. PGC) and SMS (i.e. SGC), before and after dry-wet cycles. Furthermore, the bonding modes of organic molecules and geopolymer gels, as well as their evolution mechanisms during dry-wet cycles are further analyzed. The experimental results show that the addition of 2%–6% PDMS or the replacement of 5%–15% SMS can modify metakaolin-based geopolymer concrete to become hydrophobic, having resultant water contact angles ranging from 84.7° to 139.0°. The water absorption and chloride transport rates of modified concrete also significantly decrease by up to 94.3% compared to unmodified concrete. Over 32 dry-wet cycles, PGC samples maintain efficient and unimpaired water resistance. Both the hydrophobicity and strength of PGC remain essentially unchanged, only experiencing slight decreases in water contact angle (of 4.2°–4.6°) and compressive strength (of 0.5%–2.4%). Additionally, there is no discernible increase in the presence of cracks in PGC samples. These results are attributed to the robust combination of organic hydrophobic PDMS and the geopolymer gel skeleton established through phase cross-linking.

SGC samples also demonstrate enduring hydrophobicity and strength throughout 32 dry-wet cycles, with their water contact angles and compressive strengths only decreasing 1.1°–2.3° and 1.5%–18.6%, respectively. However, compared to PGC, SGC displays less stability in long-term low water absorption during dry-wet cycles. The single water absorptions of SGC5 and SGC10 samples noticeably increase from 5.9% to 6.4% (SGC5) and from 2.5% to 4.2% (SGC10), before and after 32 dry-wet cycles. SMS micro-molecules can be combined with the gel structure in various modes, such as chemical condensation, electrostatic attraction, and physical absorption. A proportion of SMS molecules, initially adsorbed onto gels through weak binding, establishes more robust hydrogen bonds with free water molecules, thereby dissolving in the water and being transported along with it thereafter. The hydrophilic matrix where hydrophobic SMS molecules were originally attached becomes re-exposed for water adsorption. Moreover, the detachment of SMS molecules

from the gel network can result in structural damage to the matrix. As a consequence, the compressive strength of SGC10 decreases by 18.6% and its total porosity increases by 37.6% after dry-wet cycles.

Overall, both PGC and SGC can be used as long-lasting waterproof building materials. Considering the observed degradation mechanisms during dry-wet cycles, PGC presents better structural stability and higher functional performance compared to SGC. This study verifies the utility of hydrophobically-modified geopolymer concrete for long-term service in alternating wet and dry environments (e.g., buildings in areas with frequent precipitation, or structures in splash and tidal zones for coastal engineering), laying a foundation for subsequent research and applications.

Acknowledgments

This work is supported by the National Natural Science Foundation of China (Nos. 52101328 and 52171277), the National Key Research and Development Program of China (No. 2022YFE0109200), the Foundation of the Shanxi-Zheda Institute of Advanced Materials and Chemical Engineering (No. 2022SZ-TD006), and the Postdoctoral Fellowship Program of China Postdoctoral Science Foundation (CPSF) (No. GZB20230653).

Author contributions

Dongming YAN and Shengqian RUAN proposed the topic of the research. Yilu QIU and Rongfeng GAO finished the experiments. Yilu QIU processed the corresponding data and wrote the first draft of the manuscript. Shengqian RUAN and Shikun CHEN revised further and edited the final version. Dongming YAN and Yi LIU oversaw supervision, funding acquisition, and project administration.

Conflict of interest

Dongming YAN is an Editorial Board member of this journal, and is NOT involved in the editorial review or the decision to publish this article. Dongming YAN, Yilu QIU, Rongfeng GAO, Shikun CHEN, Yi LIU, and Shengqian RUAN declare that they have no conflict of interest.

References

Amran M, Al-Fakih A, Chu SH, et al., 2021. Long-term durability properties of geopolymer concrete: an in-depth review. *Case Studies in Construction Materials*, 15:e00661. https://doi.org/10.1016/j.cscm.2021.e00661

Artigas A, Monsalve A, Sipos K, et al., 2015. Development of accelerated wet–dry cycle corrosion test in marine environment for weathering steels. *Corrosion Engineering, Science and Technology*, 50(8):628-632. https://doi.org/10.1179/1743278215Y.0000000007

Babaee M, Castel A, 2018. Water vapor sorption isotherms, pore structure, and moisture transport characteristics of alkali-activated and Portland cement-based binders. *Cement and Concrete Research*, 113:99-120. https://doi.org/10.1016/j.cemconres.2018.07.006

Bakharev T, 2005. Resistance of geopolymer materials to acid attack. *Cement and Concrete Research*, 35(4):658-670. https://doi.org/10.1016/j.cemconres.2004.06.005

Banić D, Grandić D, Bjegović D, et al., 2005. Bond characteristics of corroding reinforcement in concrete beams. Application of Codes, Design and Regulations: Proceedings of the International Conference Held at the University of Dundee, p.203-210. https://doi.org/10.1680/aocdar.34037.0022

Baroghel-Bouny V, Belin P, Maultzsch M, et al., 2007. $AgNO_3$ spray tests: advantages, weaknesses, and various applications to quantify chloride ingress into concrete. Part 1: non-steady-state diffusion tests and exposure to natural conditions. *Materials and Structures*, 40(8):759-781. https://doi.org/10.1617/s11527-007-9233-1

Chandler D, 2002. Hydrophobicity: two faces of water. *Nature*, 417(6888):491. https://doi.org/10.1038/417491a

Chen SK, Ruan SQ, Zeng Q, et al., 2022. Pore structure of geopolymer materials and its correlations to engineering properties: a review. *Construction and Building Materials*, 328:127064. https://doi.org/10.1016/j.conbuildmat.2022.127064

Davidovits J, 1989. Geopolymers and geopolymeric materials. *Journal of Thermal Analysis*, 35(2):429-441. https://doi.org/10.1007/BF01904446

Duxson P, Fernández-Jiménez A, Provis JL, et al., 2007. Geopolymer technology: the current state of the art. *Journal of Materials Science*, 42(9):2917-2933. https://doi.org/10.1007/s10853-006-0637-z

Fletcher RA, Mackenzie KJD, Nicholson CL, et al., 2005. The composition range of aluminosilicate geopolymers. *Journal of the European Ceramic Society*, 25(9):1471-1477. https://doi.org/10.1016/j.jeurceramsoc.2004.06.001

Fu Q, Xu WR, Zhao X, et al., 2021. The microstructure and durability of fly ash-based geopolymer concrete: a review. *Ceramics International*, 47(21):29550-29566. https://doi.org/10.1016/j.ceramint.2021.07.190

Guo XL, Shi HS, Dick WA, 2010. Compressive strength and microstructural characteristics of class C fly ash geopolymer. *Cement and Concrete Composites*, 32(2):142-147. https://doi.org/10.1016/j.cemconcomp.2009.11.003

Hall C, 1989. Water sorptivity of mortars and concretes: a review. *Magazine of Concrete Research*, 41(147):51-61. https://doi.org/10.1680/macr.1989.41.147.51

Homan L, Ababneh AN, Xi YP, 2016. The effect of moisture transport on chloride penetration in concrete. *Construction and Building Materials*, 125:1189-1195. https://doi.org/10.1016/j.conbuildmat.2016.08.124

Israelachvili JN, 1974. The nature of van der Waals forces. *Contemporary Physics*, 15(2):159-178. https://doi.org/10.1080/00107517408210785

Jin HS, Liu J, Zhong DJ, et al., 2023. Experimental study on chloride ion diffusion behavior and microstructure in concrete under alternating ambient humidity conditions. *Construction and Building Materials*, 401:132886. https://doi.org/10.1016/j.conbuildmat.2023.132886

Kang X, Li Y, Ma XY, et al., 2022. Fabrication and characterization of high performance superhydrophobic organosilane-coated fly ash composites with novel micro–nano-hierarchy roughness. *Journal of Materials Science*, 57(29):13914-13927. https://doi.org/10.1007/s10853-022-07473-5

Khale D, Chaudhary R, 2007. Mechanism of geopolymerization and factors influencing its development: a review. *Journal of Materials Science*, 42(3):729-746. https://doi.org/10.1007/s10853-006-0401-4

Kou SC, Poon CS, 2013. Long-term mechanical and durability properties of recycled aggregate concrete prepared with the incorporation of fly ash. *Cement and Concrete Composites*, 37:12-19. https://doi.org/10.1016/j.cemconcomp.2012.12.011

Law DW, Adam AA, Molyneaux TK, et al., 2015. Long term durability properties of class F fly ash geopolymer concrete. *Materials and Structures*, 48(3):721-731. https://doi.org/10.1617/s11527-014-0268-9

Li XD, Wang Q, Lei LL, et al., 2021. Amphiphobic concrete with good oil stain resistance and anti-corrosion properties used in marine environment. *Construction and Building Materials*, 299:123945. https://doi.org/10.1016/j.conbuildmat.2021.123945

Liu HW, Liu C, Bai GL, et al., 2020. Study on the effect of chloride ion ingress on the pore structure of the attached mortar of recycled concrete coarse aggregate. *Construction and Building Materials*, 263:120123. https://doi.org/10.1016/j.conbuildmat.2020.120123

Lu SY, Wang MR, He PG, et al., 2023. Effect of sodium methylsilicate on the performance and structure of geopolymer. *Materials Letters*, 350:134893. https://doi.org/10.1016/j.matlet.2023.134893

Lv XS, Qin Y, Liang H, et al., 2022. Potassium methyl silicate (CH_5SiO_3Na) assisted activation and modification of alkali-activated-slag-based drying powder coating for protecting cement concrete. *Construction and Building Materials*, 326:126858. https://doi.org/10.1016/j.conbuildmat.2022.126858

Mastali M, Kinnunen P, Dalvand A, et al., 2018. Drying shrinkage in alkali-activated binders–a critical review. *Construction and Building Materials*, 190:533-550. https://doi.org/10.1016/j.conbuildmat.2018.09.125

MOHURD (Ministry of Housing and Urban-Rural Development of the People's Republic of China), 2010. Standard for Evaluation of Concrete Compressive Strength, GB/T 50107-2010. MOHURD, Beijing, China (in Chinese).

MWRC (Ministry of Water Resources of the People's Republic of China), 2020. Test Code for Hydraulic Concrete, SL/T 352-2020. MWRC, Beijing, China (in Chinese).

NCF (Nordic Concrete Federation), 1999. Chloride Migration Coefficient from Non-Steady-State Migration Experiments, NT Build 492. NCF, Northern Europe.

Neithalath N, Sumanasooriya MS, Deo O, 2010. Characterizing pore volume, sizes, and connectivity in pervious concretes for permeability prediction. *Materials Characterization*, 61(8):802-813. https://doi.org/10.1016/j.matchar.2010.05.004

Parbhoo B, Nagy O, 1988. Molecular dynamics in hydrogen bond forming environments. The role of hydrophilic-hydrophobic interactions in pyridine-water mixtures. *Journal of Molecular Structure*, 177:393-399. https://doi.org/10.1016/0022-2860(88)80104-2

Peng H, Yang YW, Ge YP, et al., 2022. Metakaolin-based geopolymer features different pore structure characteristics from ordinary Portland cement paste: a mechanistic study. *Journal of Materials in Civil Engineering*, 34(12):4022321. https://doi.org/10.1061/(ASCE)MT.1943-5533.0004485

Pradhan P, Dwibedy S, Pradhan M, et al., 2022. Durability characteristics of geopolymer concrete–progress and perspectives. *Journal of Building Engineering*, 59:105100. https://doi.org/10.1016/j.jobe.2022.105100

Provis JL, van Deventer JSJ, 2009. Geopolymers: Structures, Processing, Properties and Industrial Applications. Woodhead, UK, p.464.

Provis JL, Bernal SA, 2014. Geopolymers and related alkali-activated materials. *Annual Review of Materials Research*, 44(1):299-327. https://doi.org/10.1146/annurev-matsci-070813-113515

Ruan SQ, Chen SK, Zhu XY, et al., 2021. Matrix wettability and mechanical properties of geopolymer cement-polydimethylsiloxane (PDMS) hybrids. *Cement and Concrete Composites*, 124:104268. https://doi.org/10.1016/j.cemconcomp.2021.104268

Ruan SQ, Yan DM, Chen SK, et al., 2022a. Process and mechanisms of multi-stage water sorptivity in hydrophobic geopolymers incorporating polydimethylsiloxane. *Cement and Concrete Composites*, 128:104460. https://doi.org/10.1016/j.cemconcomp.2022.104460

Ruan SQ, Chen SK, Lu JY, et al., 2022b. Waterproof geopolymer composites modified by hydrophobic particles and polydimethylsiloxane. *Composites Part B: Engineering*, 237:109865. https://doi.org/10.1016/j.compositesb.2022.109865

Ruan SQ, Chen SK, Liu Y, et al., 2023a. Early-age deformation of hydrophobized metakaolin-based geopolymers. *Cement and Concrete Research*, 169:107168. https://doi.org/10.1016/j.cemconres.2023.107168

Ruan SQ, Qiu YL, Gao RF, et al., 2023b. Effect of organosilicone on the reaction process of functionalized geopolymers.

Journal of Building Engineering, 76:107348. https://doi.org/10.1016/j.jobe.2023.107348

Ruan SQ, Chen SK, Zhang YJ, et al., 2023c. Molecular-level hybridized hydrophobic geopolymer ceramics for corrosion protection. *Chemistry of Materials*, 35(4):1735-1744. https://doi.org/10.1021/acs.chemmater.2c03522

SAC (Standardization Administration of the People's Republic of China), 2020. Test Methods of Autoclaved Aerated Concrete, GB/T 11969-2020. SAC, Beijing, China (in Chinese).

She YS, Chen YX, Li LJ, et al., 2023. Understanding the generation and evolution of hydrophobicity of silane modified fly ash/slag based geopolymers. *Cement and Concrete Composites*, 142:105206. https://doi.org/10.1016/j.cemconcomp.2023.105206

Sun DW, Wang YL, Ma WX, et al., 2021. C–S–H gel structure and water molecules behaviors under different chemical environments in a range of temperatures. *Materials Today Communications*, 26:101866. https://doi.org/10.1016/j.mtcomm.2020.101866

Tang DS, Yang CH, Shen C, et al., 2023. Preparing hydrophobic alkali-activated slag mortar with lotus-leaf-like microstructure by adding polydimethylsiloxane (PDMS). *Construction and Building Materials*, 409:134148. https://doi.org/10.1016/j.conbuildmat.2023.134148

Tian ZN, Zhang ZQ, Tang XM, et al., 2023. Understanding the effect of moisture on interfacial behaviors of geopolymer-aggregate interaction at molecular level. *Construction and Building Materials*, 385:131404. https://doi.org/10.1016/j.conbuildmat.2023.131404

Tomar AS, Gupta R, Bijanu A, et al., 2023. TiO_2-geopolymer based novel corrosion protective micro-coatings to emaciate mild steel oxidation in severe environments. *Construction and Building Materials*, 395:132252. https://doi.org/10.1016/j.conbuildmat.2023.132252

Villagrán Zaccardi YA, Alderete NM, de Belie N, 2017. Improved model for capillary absorption in cementitious materials: progress over the fourth root of time. *Cement and Concrete Research*, 100:153-165. https://doi.org/10.1016/j.cemconres.2017.07.003

Wang FJ, Lei S, Ou JF, et al., 2020. Effect of PDMS on the waterproofing performance and corrosion resistance of cement mortar. *Applied Surface Science*, 507:145016. https://doi.org/10.1016/j.apsusc.2019.145016

Wang Y, Ueda T, Gong FY, et al., 2019. Meso-scale mechanical deterioration of mortar due to sodium chloride attack. *Cement and Concrete Composites*, 96:163-173. https://doi.org/10.1016/j.cemconcomp.2018.11.021

Wasim M, Ngo TD, Law D, 2021. A state-of-the-art review on the durability of geopolymer concrete for sustainable structures and infrastructure. *Construction and Building Materials*, 291:123381. https://doi.org/10.1016/j.conbuildmat.2021.123381

Witkowski H, Koniorczyk M, 2018. New sampling method to improve the reliability of FTIR analysis for self-compacting concrete. *Construction and Building Materials*, 172:196-203. https://doi.org/10.1016/j.conbuildmat.2018.03.216

Wu YG, Lu BW, Bai T, et al., 2019. Geopolymer, green alkali activated cementitious material: synthesis, applications and challenges. *Construction and Building Materials*, 224:930-949. https://doi.org/10.1016/j.conbuildmat.2019.07.112

Xie JH, Wei MW, Huang PY, et al., 2019. Fatigue behavior of the basalt fiber-reinforced polymer/concrete interface under wet-dry cycling in a marine environment. *Construction and Building Materials*, 228:117065. https://doi.org/10.1016/j.conbuildmat.2019.117065

Xue X, Liu YL, Dai JG, et al., 2018. Inhibiting efflorescence formation on fly ash-based geopolymer via silane surface modification. *Cement and Concrete Composites*, 94:43-52. https://doi.org/10.1016/j.cemconcomp.2018.08.013

Yang JX, She W, Zuo WQ, et al., 2021. Rational application of nano-SiO_2 in cement paste incorporated with silane: counterbalancing and synergistic effects. *Cement and Concrete Composites*, 118:103959. https://doi.org/10.1016/j.cemconcomp.2021.103959

Zhang DR, Zhu HJ, Wu QS, et al., 2023. Investigation of the hydrophobicity and microstructure of fly ash-slag geopolymer modified by polydimethylsiloxane. *Construction and Building Materials*, 369:130540. https://doi.org/10.1016/j.conbuildmat.2023.130540

Zhang M, Xu HY, Phalé Zeze AL, et al., 2022. Coating performance, durability and anti-corrosion mechanism of organic modified geopolymer composite for marine concrete protection. *Cement and Concrete Composites*, 129:104495. https://doi.org/10.1016/j.cemconcomp.2022.104495

Zhang P, Zheng YX, Wang KJ, et al., 2018. A review on properties of fresh and hardened geopolymer mortar. *Composites Part B: Engineering*, 152:79-95. https://doi.org/10.1016/j.compositesb.2018.06.031

Zhang ZH, Provis JL, Ma X, et al., 2018. Efflorescence and subflorescence induced microstructural and mechanical evolution in fly ash-based geopolymers. *Cement and Concrete Composites*, 92:165-177. https://doi.org/10.1016/j.cemconcomp.2018.06.010

Zhong WL, Fan LF, Zhang YH, 2022a. Experimental research on the dynamic compressive properties of lightweight slag based geopolymer. *Ceramics International*, 48(14):20426-20437. https://doi.org/10.1016/j.ceramint.2022.03.328

Zhong WL, Zhang YH, Fan LF, et al., 2022b. Effect of PDMS content on waterproofing and mechanical properties of geopolymer composites. *Ceramics International*, 48(18):26248-26257. https://doi.org/10.1016/j.ceramint.2022.05.306

Zhong WL, Qiu B, Zhang YH, et al., 2023. Mesoscopic damage characteristics of hydrophobicity-modified geopolymer composites under freezing-thawing cycles based on CT

scanning. *Composite Structures*, 326:117637. https://doi.org/10.1016/j.compstruct.2023.117637

Zhu C, Liu XG, Liu C, et al., 2022. Study on the chloride ion transport mechanism of recycled mixed aggregate concrete based on evolution characteristics of pore structure. *Construction and Building Materials*, 353:129101. https://doi.org/10.1016/j.conbuildmat.2022.129101

Zhu ZD, Huo WW, Sun H, et al., 2023. Correlations between unconfined compressive strength, sorptivity and pore structures for geopolymer based on SEM and MIP measurements. *Journal of Building Engineering*, 67:106011. https://doi.org/10.1016/j.jobe.2023.106011